

Kinesin-8 Motors Act Cooperatively to Mediate Length-Dependent Microtubule Depolymerization

Vladimir Varga,^{1,2} Cecile Leduc,^{1,2,3} Volker Bormuth,¹ Stefan Diez,¹ and Jonathon Howard^{1,*}

¹Max Planck Institute of Molecular Cell Biology and Genetics, Pfotenhauerstrasse 108, 01307 Dresden, Germany

²These authors contributed equally to this work

³Present address: CPMOH-Université Bordeaux 1, 351 Cours de la Libération, 33405 Talence, France

*Correspondence: howard@mpi-cbg.de

DOI 10.1016/j.cell.2009.07.032

SUMMARY

Motor proteins in the kinesin-8 family depolymerize microtubules in a length-dependent manner that may be crucial for controlling the length of organelles such as the mitotic spindle. We used single-molecule microscopy to understand the mechanism of length-dependent depolymerization by the budding yeast kinesin-8, Kip3p. We found that after binding at a random position on a microtubule and walking to the plus end, an individual Kip3p molecule pauses there until an incoming Kip3p molecule bumps it off. Kip3p dissociation is accompanied by removal of just one or two tubulin dimers (on average). Such a cooperative mechanism leads to a depolymerization rate that is proportional to the flux of motors to the microtubule end and accounts for the length dependence of depolymerization. This type of feedback between length and disassembly may serve as a model for understanding how an ensemble of molecules can measure and control polymer length.

INTRODUCTION

The sizes of organelles are relatively constant in cells of a given type. This is remarkable for dynamic organelles—such as axonemes, microvilli, and mitotic spindles—whose molecules exchange with those in the cytoplasm on the timescale of minutes to days (Taylor and Wang, 1980; Wadsworth and Sloboda, 1983). In such organelles, exchange takes place by polymerization and depolymerization of the constituent cytoskeletal filaments, and the overall length depends on the balance of these processes (Marshall et al., 2005; Goshima et al., 2005). Because polymerization and depolymerization take place exclusively at the filament ends, control of organelle size must involve feedback between the filament length and the growth/shrinkage dynamics; the feedback must have negative sign in the sense that a longer filament leads to a lower polymerization rate or a higher depolymerization rate. With such feedback, a balance between polymerization and depolymerization will be achieved

at a unique filament length (Marshall, 2004; Howard and Hyman, 2007; Gardner et al., 2008).

An example of tight size regulation is the mitotic spindle. In *Drosophila* S2 cells, the length of the spindle at metaphase varies little from cell to cell ($11.5 \pm 2.0 \mu\text{m}$, mean \pm standard deviation [SD], Goshima et al., 2005). Many proteins are involved in modulating spindle length. For example, reducing the levels of the polymerase Msps (chTOG/XMAP215) and other plus-tip proteins by RNAi decreases spindle lengths, whereas reducing the levels of depolymerases such as Kip10A (kinesin-13) and Kip67A (kinesin-8) increases spindle lengths (Goshima et al., 2005). Interfering with depolymerizing kinesins also increases spindle size in yeast (Straight et al., 1998) and human cells (Mayr et al., 2007). Overexpressing these proteins has the opposite effect to reducing their levels (Goshima et al., 2005). However, which of these microtubule-regulating proteins control length—meaning that they provide the feedback between length and filament dynamics—and which simply modulate length is not known.

Recently, we discovered, using an assay with purified proteins, that the budding yeast kinesin-8, Kip3p, depolymerizes longer microtubules faster than shorter microtubules (Varga et al., 2006). Similar activity was reported for a human homolog (Mayr et al., 2007). These experiments were done on stabilized microtubules, a model for the GTP cap that regulates the catastrophic conversion of a growing microtubule to a shrinking one, suggesting that kinesin-8s induce length-dependent catastrophes of dynamic microtubules. For the fission yeast homologs, no depolymerization activity has been observed *in vitro* (Grissom et al., 2009), but *in vivo* they have been shown to promote catastrophes (Unsworth et al., 2008) and do so in a length-dependent manner (Tischer et al., 2009). Thus, kinesin-8s are not just modulators of filament dynamics, but may provide the negative feedback needed to control the lengths of microtubules and thereby microtubule-containing structures like the mitotic spindle. Testing this hypothesis in cells requires more refined experiments than simple alterations of protein levels: it requires replacement by proteins whose depolymerization properties have been altered such that the length dependence is changed in predictable ways. A prerequisite of such experiments is an understanding of the molecular mechanisms underlying length control. This is the goal of the present paper. Moreover, length-dependent depolymerization is a fascinating problem in itself: how do molecules that are

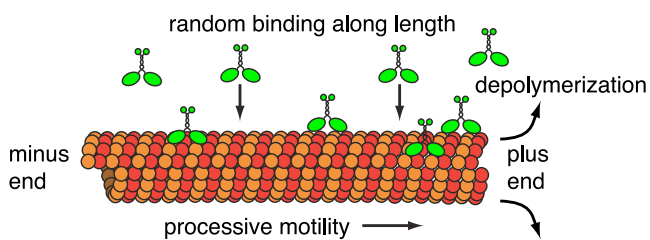


Figure 1. Antenna Model

Motor molecules land randomly on the microtubule lattice. Consequently, the number of landings in a given time interval is proportional to the microtubule's length. The high processivity of movement assures that almost all motors reach the plus end of the microtubule, where they cause depolymerization. The net result is that longer microtubules depolymerize more quickly.

only a few tens of nanometers in diameter know to depolymerize a 10 μm -long microtubule faster than a 5 μm -long microtubule, when both microtubules are hundreds of times larger than the dimensions of Kip3p?

One possible model for length-dependent depolymerization is the antenna model shown in Figure 1 (Varga et al., 2006). According to this model, motor molecules bind randomly along the length of the microtubule and their high processivity funnels them to the plus end, leading to depolymerization. The model predicts that the motors form a concentration gradient along a microtubule (increasing toward the plus end), as has been observed for kinesin-8 in vitro (Varga et al., 2006) and in vivo (Stumpff et al., 2008). Recently, it has been proposed that kinesin-5 uses a similar mechanism to control the lengths of kinetochore microtubules in budding yeast (Gardner et al., 2008).

In this paper, we have used total-internal-reflection-fluorescence (TIRF) microscopy to critically test the antenna model and understand the molecular mechanism of the actual depolymerization event mediated by Kip3p. By directly observing the behavior of individual Kip3p molecules on microtubules over a wide range of Kip3p concentrations, we found that an individual Kip3p molecule remains stationary at the plus end, and that its dissociation is greatly accelerated by incoming Kip3p molecules. Dissociation is accompanied by removal of just one or two tubulin dimers. Incorporation of this mechanism into a mathematical formulation of the antenna model allowed us to account quantitatively for the length dependence of depolymerization.

RESULTS

Observing Single Kip3p Molecules at High Concentrations Requires Spiking Experiments

To understand how Kip3p shortens microtubules, we needed to study the interactions of individual Kip3p molecules with the microtubule lattice and ends over a wide range of Kip3p concentrations. However, a limitation of single-molecule fluorescence experiments is that they can only be performed at low concentrations because otherwise there are too many fluorescent molecules to be able to resolve the individual ones. To overcome this limitation, we performed spiking experiments. In these experiments, the concentration of Kip3p-EGFP was kept low (<0.1 nM) so that individual fluorescent Kip3p molecules interacting with GMPCPP-

stabilized, rhodamine-labeled microtubules could be detected by TIRF microscopy. To increase the total Kip3p concentration, we then added variable amounts of unlabeled Kip3p.

The End-Residence Time of Kip3p Depends on the Total Kip3p Concentration

Spiking experiments revealed an unusual interaction between Kip3p molecules at the microtubule end. At low total Kip3p concentrations (<0.1 nM), single Kip3p-EGFP molecules attached to the microtubules and moved processively with a velocity of $3.2 \pm 0.3 \mu\text{m}/\text{min}$ (SD, N = 67) and with a run length of $11 \pm 2 \mu\text{m}$ (standard error of the mean [SEM], N = 26 dissociations that occurred before the molecules reached the plus end) toward the microtubule plus ends. There, they remained for $36 \pm 4 \text{ s}$ (SEM, N = 46) before dissociating (Figure S1 available online). An example is shown in Figure 2A; end pausing is seen on all microtubules (Figure S2). At these low Kip3p concentrations, the depolymerization rate at the plus ends was $\sim 0.015 \mu\text{m}/\text{min}$, similar to the spontaneous depolymerization measured in the absence of Kip3p. When the total Kip3p concentration was increased by adding unlabeled Kip3p to give a depolymerization rate of $\sim 0.1 \mu\text{m}/\text{min}$, we measured a similar walking velocity of $2.7 \pm 0.4 \mu\text{m}/\text{min}$ (SD, N = 36) and a similar processivity of $13 \pm 5 \mu\text{m}$ (SEM, N = 8). However, remarkably, the end-residence time decreased ~ 3 -fold to $\sim 10 \text{ s}$ (Figure 2B). When the total Kip3p concentration was increased further to give a depolymerization rate of $\sim 1 \mu\text{m}/\text{min}$, the walking velocity ($3.0 \pm 0.4 \mu\text{m}/\text{min}$, SD, N = 40) and run length ($10 \pm 3 \mu\text{m}$, SEM, N = 14) again remained almost unchanged. But the end-residence time decreased even further to $< 3.5 \text{ s}$ (Figure 2C and Movie S1). Thus, the end-residence time decreases as the total concentration of Kip3p increases. This indicates that Kip3p molecules influence each other at the microtubule ends.

The End-Residence Time of Kip3p Inversely Correlates with the Depolymerization Rate

As the total Kip3p concentration was increased, the depolymerization rate increased. Because all protofilaments must be depolymerizing at the same average rate, we can determine an average lifetime of the terminal tubulin dimers at the microtubule end from the depolymerization rate (using the fact that the tubulin dimer has a length of 8.4 nm; Hyman et al., 1995). A plot of the Kip3p end-residence time against this average lifetime (200 molecules on 31 microtubules) was well fitted by a straight line (Figure 2D). The y-intercept was $2.1 \pm 0.5 \text{ s}$ (SEM), consistent with a small bias due to the minimum frame rate of 3.0 s for these experiments. The slope was 1.00 ± 0.08 (SEM), indicating that on average one tubulin dimer dissociated for each Kip3p that dissociated. This value of the stoichiometry of the Kip3p depolymerase activity (i.e., the number of tubulin dimers removed per Kip3p) is a slight underestimate due to photobleaching of Kip3p-EGFP at the ends. The underestimate is by about 5%, calculated from the average bleaching time of 400 to 600 s at the frame rates used.

The Depolymerization Rate Linearly Correlates with the Flux of Kip3p to the Plus End

A second, independent way to estimate the stoichiometry of Kip3p is to divide the number of tubulin dimers that dissociate

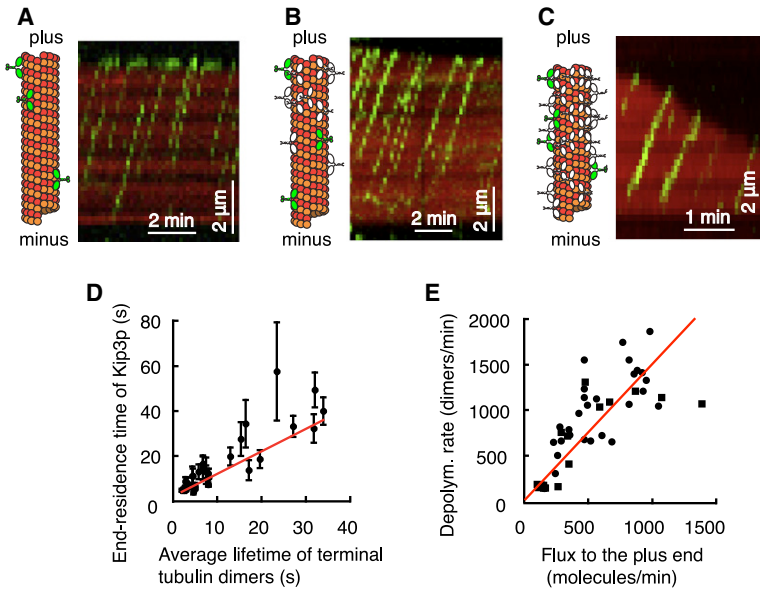


Figure 2. Determination of the Kip3p Depolymerization Stoichiometry from Spiking Experiments

(A–C) Kymographs of single Kip3p-EGFP molecules (green) imaged by TIRF microscopy on microtubules (red) in the presence of varying amounts of unlabeled Kip3p molecules (white motors in the schematics). (A) 0.05 nM Kip3p-EGFP, 0 nM unlabeled Kip3p, 1 frame per 10 s. (B) 0.05 nM Kip3p-EGFP, 2.9 nM unlabeled Kip3p, 1 frame per 10 s. (C) 0.03 nM Kip3p-EGFP, 5.1 nM unlabeled Kip3p, 1 frame per 3.5 s. (See also Movie S1).

(D) End-residence time of Kip3p-EGFP (mean \pm SEM, each point is from one microtubule) versus average lifetime of the terminal tubulin dimers (calculated from the depolymerization rate). The red line corresponds to a stoichiometry of 1.0.

(E) Average depolymerization rates (expressed as tubulin dimers per minute) versus flux of Kip3p to the microtubule plus ends. The different symbols denote two different Kip3p-EGFP preparations. The red line corresponds to a stoichiometry of 1.5.

from the end by the number of Kip3p that arrive at the end. We counted the numbers of Kip3p-EGFP molecules that reached the plus ends in a given time interval and calculated the flux of Kip3p-EGFP to the ends. This Kip3p-EGFP flux was then multiplied by the ratio of the total Kip3p concentration to the concentration of Kip3p-EGFP to estimate the total flux of Kip3p to the microtubule ends. We found that the total flux was strongly correlated with the microtubule depolymerization rate expressed as the number of tubulin dimers dissociating from the end of a microtubule per minute (Figure 2E). We fitted a line through these data with a y -intercept fixed at 26 tubulin dimers per minute (corresponding to the spontaneous depolymerization rate of 0.015 $\mu\text{m}/\text{min}$). The slope of the line was 1.47 ± 0.08 (SEM, $N = 450$ Kip3p-EGFP molecules on 45 microtubules), with an additional error of $\sim 10\%$ arising from uncertainty in the ratio of labeled to unlabeled Kip3p. This value of the stoichiometry is overestimated by about 20% due to photobleaching of molecules moving on the lattice. We conclude that each Kip3p molecule arriving at the end causes the dissociation of (on average) one to two tubulin dimers.

The Kinetics of Microtubule Length Changes Can Be Quantitatively Described by the Antenna Model

The observed linearity between the flux of Kip3p to the plus end and the depolymerization rate provided the crucial information needed to formulate the antenna model mathematically. Because the total rate of Kip3p landing on a microtubule is proportional to its length (Figure S3) and the processivity is very high (most motors that bind reach the end), we can predict both the time course of microtubule shortening and the density of Kip3p along the microtubule lattice (Supplemental Data). The depolymerization rate, ν_- , of a microtubule of length L is the product of the flux of Kip3p molecules to the end and the distance the microtubule shortens per Kip3p arrival at the end. The flux is $\rho(L)(\nu_+ + \nu_-)$, where $\rho(L)$ is the density of Kip3p at the end of the

microtubule and ν is the velocity of movement of Kip3p along the microtubule. Note that the flux is proportional to the sum of the rate at which the motors move to the plus ends and the rate at which the plus ends move to the motors. The shortening distance is equal to nd , where n is the number of tubulin dimers removed per Kip3p molecule (the stoichiometry), and d is the change of microtubule length corresponding to the removal of one tubulin dimer ($d = 0.6 \text{ nm}$ equals the tubulin dimer length, 8.4 nm, divided by the number of protofilaments in GMPCPP microtubules, 14, Hyman et al., 1995). This gives $\nu_- = \nu nd \rho(L) / [1 - nd \rho(L)]$ (see Supplemental Data for a full derivation).

To compare the predictions of the model to the experimental data, we simultaneously measured the length of the rhodamine-labeled microtubules and the density of Kip3p-EGFP molecules (in experiments where no unlabeled motors were added), using epifluorescence and TIRF microscopy, respectively. For these experiments, it was crucial to keep the concentration of Kip3p-EGFP in solution constant over time, i.e., to minimize sequestering effects of Kip3p-EGFP by the microtubules. To alleviate this problem, we used large-volume chambers (depth 400 μm instead of the usual 100 μm) and a low density of microtubules (2–5 microtubules per $80 \times 80 \mu\text{m}^2$). Figure 3A shows a kymograph of a microtubule depolymerizing under these conditions.

Two phases of depolymerization were observed. Phase (i) corresponds to an acceleration phase during which a linear density profile of Kip3p-EGFP along the microtubule toward the plus end is being built up (Figure S4A). The density profile accords with the model: at early times (t) after addition of Kip3p, the density increases linearly with distance (x) from the minus end ($\rho(x) = rx/\nu$, $x \leq \nu t$), where r is the landing rate of Kip3p per unit length of the microtubule lattice, and then remains at a constant value ($\rho(x) = rt$) until the plus end. This phase finishes when the density profile is fully established and the depolymerization rate reaches its maximum. Phase (ii) corresponds to a slow-down phase during which the density

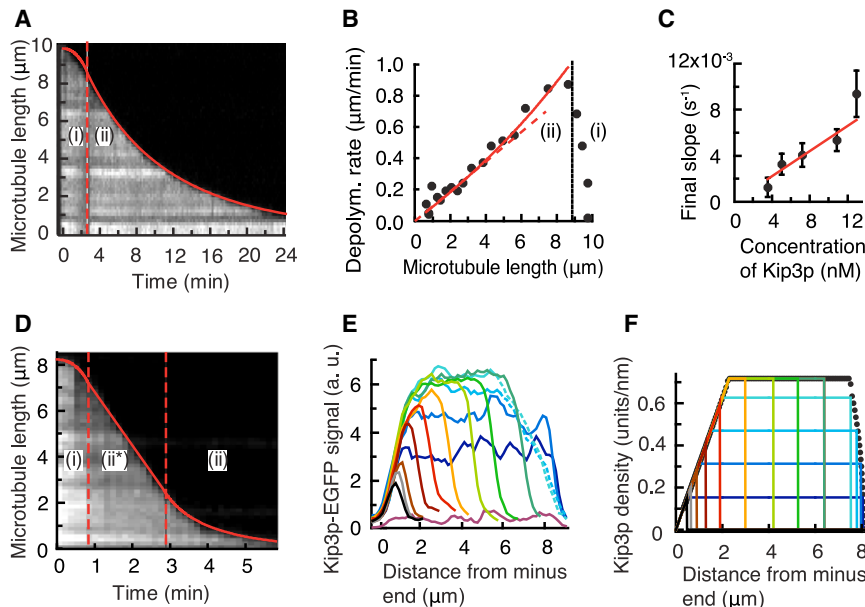


Figure 3. Microtubule Depolymerization Rates and Kip3p Densities Are Well Fit by the Antenna Model

(A) Kymograph of a microtubule depolymerized by 1.2 nM Kip3p-EGFP. Images were recorded every 10 s. The solid red line denotes a fit to the model for phases (i) and (ii) (see text and [Supplemental Data](#) for the equations).

(B) Depolymerization rate versus microtubule length for the microtubule depicted in (A). The solid red line denotes a fit to the model for phase (ii). The dashed line denotes the slope at microtubule length equal to zero ("final slope").

(C) Plot of the final slope (mean \pm SEM, 5 microtubules at each concentration) versus concentration of Kip3p. The solid red line denotes a fit (weighted by the SEM) to the model.

(D) Kymograph of a microtubule depolymerized by 1.8 nM Kip3p-EGFP. The images were recorded every 10 s. The solid red line is a fit to the model for the three depolymerization phases.

(E) Plots of the EGFP intensities, along the microtubule shown in (D), at different times after injection of Kip3p-EGFP. Time increases from magenta (0 s) in 10 s intervals through dark blue to aquamarine (0 s) in 30 s intervals to black. Black dots indicate the position of the microtubule plus end at 2.5 s intervals.

rine (40 s) and then in 30 s intervals to black. Regions where part of the microtubule was not completely resolved in TIRF due to being out of focus are shown as dashed lines.

(F) Theoretically predicted Kip3p densities along the microtubule lattice. Time increases in 10 s intervals from dark blue to aquamarine and then in 30 s intervals to black. Black dots indicate the position of the microtubule plus end at 2.5 s intervals.

profile of Kip3p-EGFP does not change over time, but the maximum Kip3p-EGFP density at the plus end decreases due to microtubule shortening ([Figure S4B](#)). This also accords with the model, which predicts that the density at the plus end is $\rho(L) = rL/v$. The change in length of the microtubule over time during both phases is well accounted for by the model (solid red curve in [Figure 3A](#)). Importantly, during phase (ii) there is an approximately linear relation between the depolymerization rate and microtubule length ([Figure 3B](#)).

The theoretical model allowed the stoichiometry to be estimated by a third method. The slope of the depolymerization rate versus microtubule length at microtubule length equal to zero (denoted "final slope," red dashed line in [Figures 3B](#) and [S5A](#)) is $n\mu$. By counting the landings of Kip3p-EGFP molecules on microtubules, we measured an association rate constant ($r/[Kip3p]$) of 24 ± 3 nM⁻¹·min⁻¹·μm⁻¹ (SEM, 65 Kip3p-EGFP molecules landing on 6 microtubules). From the final slope measured at different Kip3p concentrations ([Figure 3C](#)), we obtained an estimate of the stoichiometry, 2.3 ± 0.4 (SEM). This estimate is not affected by photobleaching.

At High Kip3p Concentrations the Depolymerization Rate Saturates

At high concentrations of Kip3p (Kip3p-EGFP or unlabeled), we observed a third depolymerization phase (ii*), between the acceleration phase (i) and the slow-down phase (ii), during which the depolymerization rate remained fixed at its maximum value ([Figures 3D](#), [S5A](#), and [S5B](#)). Several lines of evidence suggest that this saturation of the depolymerization rate was due to the limited number of Kip3p-binding sites on the microtubule lattice. First, when using Kip3p-EGFP, we observed that the motor density toward the plus end was saturated ([Figure 3E](#) between

$t = 40$ s and 160 s). Second, we observed that the maximum depolymerization rate measured during the saturation phase was independent of the initial microtubule length ([Figures S5B](#) and [S5C](#)) and approximately independent of the Kip3p concentration (data not shown). And third, our model, which took into account the limited number of motor-binding sites on the microtubule lattice, provided a good fit to the whole depolymerization curve including the saturation phase (ii*) (red line, [Figure 3D](#)) and also quantitatively predicted the measured density profiles of Kip3p (compare [Figure 3E](#) with [Figure 3F](#)) and the depolymerization rates ([Figure S5A](#)).

The Highest Depolymerization Rates Are Similar to the Velocity of Kip3p Molecules

The highest depolymerization rates measured during the saturation phases ranged from 2.5 to 4 μm/min in different experiments. This is similar to the velocity of movement of individual Kip3p-EGFP molecules measured under single-molecule conditions (3.2 ± 0.3 μm/min). This gives additional insight into the stoichiometry. The antenna model predicts that during the saturation phase, the depolymerization rate is $v_{max}^* = vnd\rho_{max}/(1 - nd\rho_{max})$, where $d\rho_{max}$ is the fraction of the microtubule lattice occupied by Kip3p at saturation ($d\rho_{max} = 0.5$ corresponds to one Kip3p dimer per two tubulin dimers). Thus, the depolymerization rate diverges as $nd\rho_{max}$ approaches unity (this is because the faster the depolymerization rate the higher the flux to the end due to the end shortening). However, our observation that the highest depolymerization rates are approximately equal to the walking velocity implies that $nd\rho_{max} \approx 0.5$. Assuming a maximum microtubule lattice occupancy, $d\rho_{max}$, of 0.25 to 0.5 as estimated by [Seitz and Surrey \(2006\)](#) for conventional kinesin in ATP, then n is between 1 and

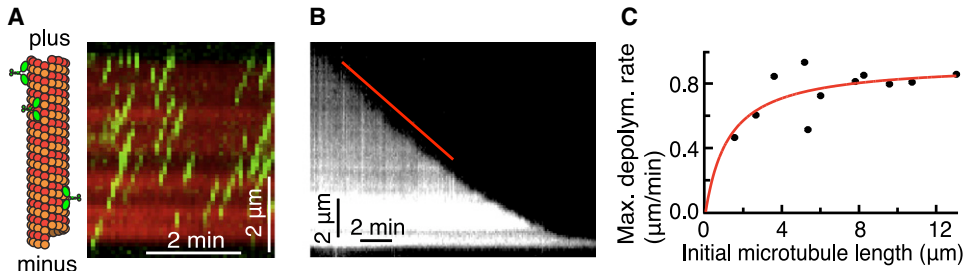


Figure 4. Increasing the Ionic Strength Decreased Processivity and Decreased the Length Dependence of Depolymerization

(A) Kymograph of single Kip3p-EGFP molecules (0.016 nM Kip3p-EGFP) moving along a microtubule in the buffer containing an additional 90 mM KCl over that in our usual buffer. Images were recorded every 5 s.

(B) Kymograph of a microtubule being depolymerized by 1.6 nM Kip3p-EGFP. Images were recorded every 5 s. The solid red line corresponds to a constant depolymerization rate of 0.8 μm/min.

(C) Maximum depolymerization rate versus initial length for 11 microtubules ranging in length from 2 to 13 μm in the presence of 1.6 nM Kip3p. The red curve reaches a maximum depolymerization rate of 0.92 μm/min; the half-maximum rate occurs at a length of 1.2 μm.

2. A strength of this last estimate of the stoichiometry is that it applies at high Kip3p concentrations (the others are more accurate at low concentrations) and is insensitive to photo-bleaching.

Length-Dependent Depolymerization Relies on High Processivity

The antenna model predicts that the depolymerization rate increases with length of the microtubule only up to a length equal to the average run length of the motors; beyond this length the depolymerization rate of the microtubule is expected to approach a plateau. This is because the “capture length” of the antenna is limited to the processivity length. Thus, the antenna model predicts that decreasing the processivity will lead to lessening of length-dependent depolymerization.

To test this prediction, we decreased the processivity of Kip3p by adding an additional 90 mM KCl to our usual buffer. The average run length in single-molecule experiments (Figure 4A) decreased about 10-fold to 1.6 ± 0.3 μm (SEM, N = 37 dissociations) and in spiking experiments to 1.2 ± 0.1 μm (SEM, N = 128 dissociations). The velocity was unchanged. In the experiment shown in Figure 4B, microtubules depolymerized at a constant rate of ~ 0.8 μm/min until they were only a few microns long, when the rate slowed (compare Figure 4B to Figure 3A). While the depolymerization rate was constant, the intensity of Kip3p-EGFP close to the plus end was constant (Figure S6). A plot of the maximum depolymerization rate against microtubule length for several microtubules showed that the rate was independent of length (for microtubules longer than a few microns) (Figure 4C). This length independence was not due to saturation of the Kip3p density because if we used a higher Kip3p concentration, a higher depolymerization rate could be obtained (data not shown). We conclude that high processivity is necessary for length-dependent depolymerization. This tests one of the key assumptions behind the antenna model.

Kip3p Is Stationary while Pausing at the Microtubule Plus End

To obtain a more detailed picture of the depolymerization event, we localized Kip3p with nanometer precision as it reached the

plus end. Because EGFP is not sufficiently photostable for long-term observation at high spatial and temporal resolution, we attached quantum dots (QDs) to the Kip3p molecules. In one arrangement, we bound streptavidin-coated QDs to the motor domain of Kip3p-EGFP using biotinylated anti-His antibodies (Figure 5A). To assure that only one Kip3p-EGFP molecule was attached to a QD, a large excess of QDs was used and the QD-motor ratio was verified using TIRF microscopy. QD-motor complexes were localized with a spatial precision of about 2 nm at a time resolution of 100 ms per frame (Leduc et al., 2007).

Figure 5B shows a typical plot of distance versus time for a QD with an attached Kip3p-EGFP molecule. The QD moved processively along the microtubule with a velocity of 3 μm/min until it reached the plus end, where it paused for 7 s. The average end-residence time of 13 QDs was 27 ± 9 s (SEM, N = 10 dissociations). When additional Kip3p was added, leading to an increase in the depolymerization rate, the end-residence time of the QDs decreased: when the average lifetime of the terminal tubulin dimers was 6 s, the average end-residence time of the QDs was 8 ± 2 s (SEM, N = 14). During the end-residence time, the mean position of the QD remained fixed. There was no indication that Kip3p was moving with the shrinking end of a microtubule as would be expected if Kip3p sequentially removed many tubulin dimers from the end.

The fluctuations of the QD around its mean position had a standard deviation of about 10 nm, much larger than the 2 nm precision of our apparatus. The fluctuations may be due to the compliance of the linkage between the QD and the attached motor domain. Another possibility is that Kip3p is rocking back and forth between tubulin dimers near the microtubule end. However, the pairwise distance histogram for 17 QDs (Figure 5C) showed no obvious peak at 16 nm, corresponding to the QD-labeled motor domain stepping back and forth between tubulin dimers on either side of the other motor domain. A peak at 8 nm, for example a labeled motor domain alternating between bound and free conformations, cannot be excluded due to the noise. The positional fluctuations imply that diffusion of Kip3p backward from the end is slow: the diffusion coefficient would be about $300 \text{ nm}^2/\text{s}$ ($= \text{SD}^2/2t$ where t is the time between forward, ATP-driven steps), about 1000 times

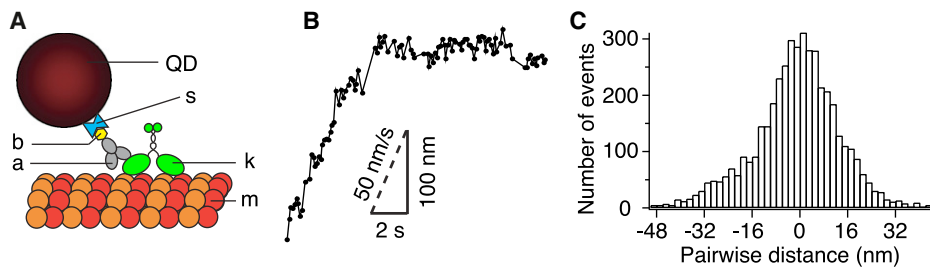


Figure 5. High-Resolution Tracking of Kip3p at the Microtubule Plus End

(A) Experimental set-up of quantum dot (QD) attachment to the motor domain of Kip3p-EGFP (s, streptavidin; b, biotin; a, anti-His antibody; k, His₆-Kip3p-EGFP; m, part of the microtubule lattice).
(B) Typical trace of tracked QD positions projected onto the axis of the microtubule. The QD moves processively along the microtubule and then remains stationary at the plus end.
(C) A pairwise distance histogram of 17 QD end-binding events shows no tendency for the Kip3p molecules to dwell at 16 nm intervals.

smaller than the diffusion of other kinesins and other microtubule-associated proteins (Cooper and Wordeman, 2009).

To check that the pausing of the QDs was not an artifact of the particular geometry of attachment of the QD to the motor or of the EGFP labeling, we performed additional control experiments: QDs were attached to the C termini of Kip3p-EGFP using biotinylated anti-GFP antibodies and to the motor domains of nonlabelled Kip3p using biotinylated anti-His antibodies. Similar results were obtained (Figures S7A and S7B).

We conclude that Kip3p pauses at the ends of microtubules for tens of seconds and does not undergo directed backward motion or random one-dimensional diffusion. These QD experiments therefore strongly support a picture in which Kip3p stays very close to the stationary microtubule end and removes only a small number of tubulin dimers.

Single-Motor Forces Accelerate Detachment of Kip3p from the Plus End

To gain information about the strength of the association of Kip3p with the microtubule end, we performed gliding assays. Kip3p-EGFP molecules were immobilized on a coverslip via anti-GFP antibodies and the gliding of rhodamine-labeled microtubules over the surface was visualized by epifluorescence microscopy. When performing the assays at low Kip3p-EGFP densities (<0.5 molecule/ μm^2 based on observations of individual motors imaged by TIRF microscopy), gliding microtubules swiveled around a single attachment point on the surface, indicative of processive movement by a single motor (Figure 6, phases 1 and 4). The mean gliding velocity was $3.2 \pm 0.3 \mu\text{m}/\text{min}$ (SD, N = 17), identical to the velocity of single Kip3p-EGFP molecules on microtubules. When the plus end of the microtubule reached the active motor, the microtubule pivoted around this attachment point (Figure 6, phase 5) for an average of $52 \pm 5 \text{ s}$ (SEM, N = 58) (Figure S8).

Occasionally, microtubules being moved by a single Kip3p-EGFP molecule got attached to a second motor. The concerted action of more than one motor was apparent from the absence of swiveling during the gliding motion (Figure 6, phase 2). When the trailing plus ends of the microtubules reached one of the active motors, the gliding ceased, presumably due to the end-bound motor acting as a brake (Figure 6, phase 3). After pausing, which lasted $27 \pm 3 \text{ s}$ (SEM, N = 11), the microtubules resumed

their movement. Concurrently, they started to swivel (again indicative of single-motor activity), and the beginning of this movement could be clearly related to the release of the end-bound motor (Figure 6, phase 4). Thus, the interaction time of Kip3p-EGFP with the plus end of a microtubule is reduced by about 50% when the microtubule is pulled away by a second, active Kip3p-EGFP molecule.

At high motor densities ($>10 \text{ molecules}/\mu\text{m}^2$) no swiveling of microtubules was observed (Movie S3), indicating that the microtubules were always attached to many motors. Consistent with multi-motor attachment, the microtubules traveled distances much longer than their lengths (Figure S9A) as seen for kinesin-1 (Howard et al., 1989). Microtubules moved slower ($1.7 \pm 0.2 \mu\text{m}/\text{min}$, SD, N = 9) than in low-density assays, indicating mutual interference when many Kip3p molecules move a single microtubule (this is unlike kinesin-1, Crevanna et al., 2008). Importantly, under these high-density conditions, no pausing was detected (Figure S9B). This shows that forces generated by several motors can accelerate the detachment of end-bound motors.

Evidence for a Direct Mechanical Interaction between Kip3p Molecules at the Microtubule End

How does the incoming Kip3p accelerate dissociation of the end-bound one? One possibility is that the incoming Kip3p destabilizes the lattice at the microtubule end, and that the reduction in end-residence time is a consequence of depolymerization. We have two lines of evidence, however, that the reduction in end-residence time does not require depolymerization.

The first line of evidence is based on experiments with microtubules stabilized by both GMPCPP and taxol. These “doubly stabilized” microtubules do not detectably depolymerize, either spontaneously or in the presence of Kip3p. Despite the absence of depolymerization, Kip3p still dissociates: the end-residence time of Kip3p-EGFP at low total Kip3p concentration was $77 \pm 5 \text{ s}$ (SEM, N = 72 molecules, Figure 7A). When the concentration of Kip3p was increased (in spiking experiments), we found that the end-residence time of Kip3p-EGFP was decreased (Figures 7B and 7C), showing that depolymerization is not necessary for Kip3p dissociation. However, depolymerization does accelerate Kip3p dissociation: at high Kip3p concentrations the average end-residence times did not decrease below 9 s (Figure 7C),

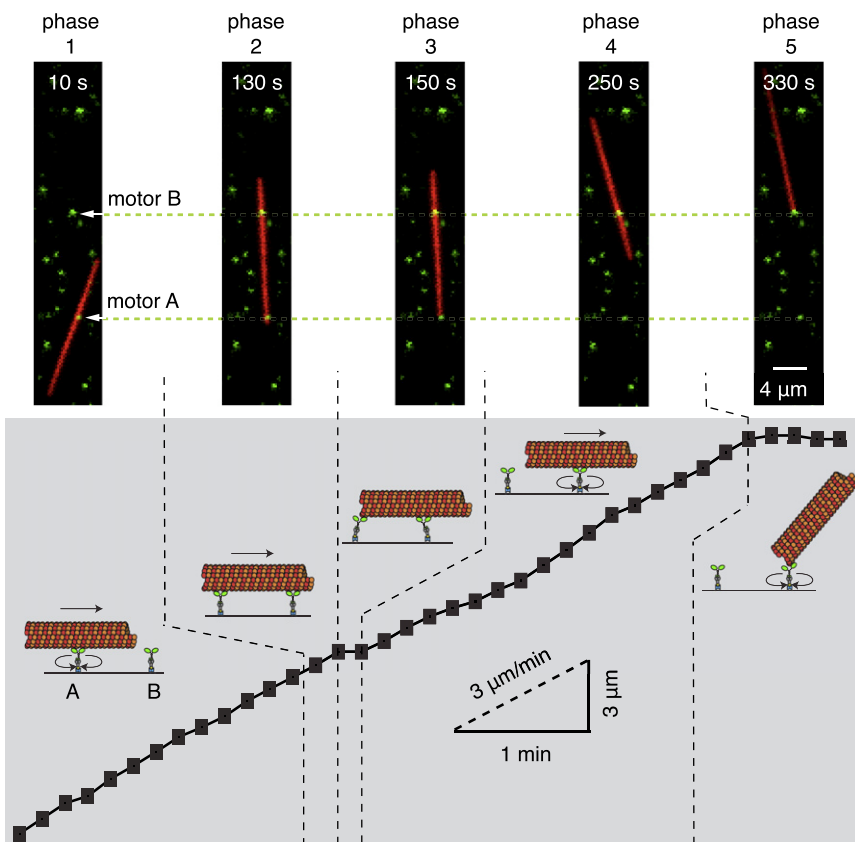


Figure 6. End Binding Can Stall the Gliding of a Microtubule across a Kip3p-Coated Surface

Micrographs of a microtubule (red) propelled by two Kip3p-EGFP molecules (green). Phase 1: the microtubule is moved by motor A. Phase 2: the microtubule is moved by both motors. Phase 3: the microtubule pauses when its plus end reaches motor A. Phase 4: the microtubule is moved by motor B (after detachment from motor A). Phase 5: the microtubule stays attached via its plus end to motor B. The lower panel shows the position of the microtubule's minus end with respect to the motors versus time. (See also Movie S2).

DISCUSSION

We have used single-molecule assays to investigate how Kip3p, the budding yeast kinesin-8, depolymerizes microtubules. The spiking experiments showed directly that (1) the total rate at which Kip3p molecules land on a microtubule is proportional to the microtubule's length, (2) Kip3p is a highly processive motor over a wide range of Kip3p densities on the microtubule lattice, and (3) the rate of depolymerization is proportional to the flux of Kip3p molecules to the microtubule end. These properties, when incorporated into a

mathematical formulation of the antenna model, are sufficient to give a length-dependent depolymerization rate. The measured time courses of microtubule depolymerization and Kip3p density profiles accord with this model. Crucially, the decrease in the total rate of Kip3p landing as a microtubule shortens leads to a decreasing depolymerization rate; this demonstrates, at the level of individual microtubules, that Kip3p is a length-dependent depolymerase (Varga et al., 2006).

Our experiments establish that a highly processive motor combined with a low-stoichiometry depolymerase (i.e., that removes a small number of tubulin dimers when it reaches the end) gives a length-dependent depolymerization over a wide range of microtubule lengths. The molecular properties of Kip3p described here make it well suited to regulating microtubule length in cells. The concentration of Kip3p in vivo is ~30 nM (700 molecules [Ghaemmaghami et al., 2003] in a volume of 20 to 40 μm^3 [Tyson et al., 1979]), though some molecules may not be active; cellular microtubules are up to several microns long. This concentration and microtubule length are similar to those used in this study and lead to a depolymerization rate that increases with length. Thus, there is sufficient Kip3p in cells to be able to regulate length.

Stoichiometry of the Depolymerase Reaction

Four different types of experiments showed that the stoichiometry of Kip3p's depolymerase activity is small: one or two. A caveat of the first three estimates is that the end-residence time or landing rates of unlabeled Kip3p may differ from labeled protein. However, the fourth estimate (from the saturation

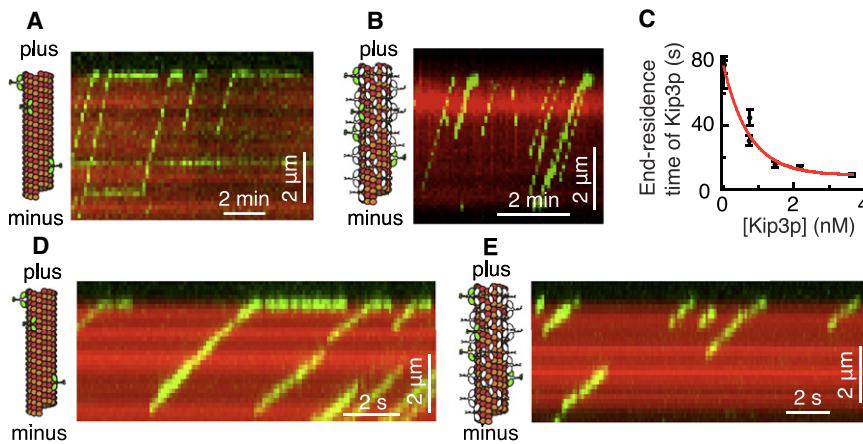
much longer than the end-residence times observed during fast depolymerization of GMPCPP microtubules (Figure 2).

Kinesin-1 Shortens the End-Residence Time of Kinesin-1 but Not that of Kip3p

A second line of evidence that dissociation of end-bound motors does not require depolymerization comes from experiments with kinesin-1. In buffers with physiological ionic strength, kinesin-1 does not dwell noticeably after it reaches the microtubule end (end-residence time < 0.3 s) (Figure S10). However, in low-ionic-strength buffer (20 mM PIPES rather than 80 mM), kinesin-1-GFP resides for 0.82 ± 0.55 s (SD, N = 43) at the end (Figures 7D and S11). In the presence of unlabeled kinesin-1, the end-residence time decreased to 0.38 ± 0.23 s (SD, N = 51) (Figures 7E and S11). Similar results were obtained in three independent experiments. The addition of kinesin-1 did not detectably increase the depolymerization rate of the GMPCPP-stabilized microtubules beyond their spontaneous depolymerization rate. Thus, the decrease in the end-residence time is not due to depolymerization.

Interestingly, in mixed motor experiments, unlabeled kinesin-1 did not decrease the end-residence time of Kip3p (Figure S12). This shows that the ability to decrease the end-residence time of Kip3p is Kip3p specific.

The reduction in end-residence time in the absence of depolymerization, seen both for Kip3p on doubly stabilized microtubules and kinesin-1 on GMPCPP microtubules, suggests that there is a direct mechanical interaction between motors at the microtubule end.



(D) Kymograph of kinesin-1-GFP molecules (green, 0.02 nM kinesin-1-GFP, 0 nM unlabeled kinesin-1) moving along a doubly stabilized microtubule in low-ionic-strength buffer. Note the expanded timescale compared to the Kip3p experiments.

(E) Kymograph showing that at high kinesin-1 concentrations (green, 0.02 nM kinesin-1-GFP, 1 nM unlabeled kinesin-1) the end-residence time of kinesin-1-GFP decreases, showing that kinesin-1 can bump itself off the end.

experiment) is not affected by this caveat as it was made under conditions where all the molecules were labeled. A stoichiometry of one is optimal because it gives length-dependent depolymerization over the widest range of active Kip3p concentrations.

Kip3p Pauses at the Plus Ends of Microtubules

A surprising finding of the TIRF experiments was that after reaching the plus end of a microtubule, Kip3p can remain there for about half a minute. This was confirmed by the high-precision QD experiments (which also showed that Kip3p remains stationary at the end) and the gliding assays (which also showed that a force similar to the motor force is needed to accelerate detachment of this paused Kip3p). The long residence time at the microtubule end likely accounts for the tip-tracking activity of Kip3p observed *in vivo* (Gupta et al., 2006; Varga et al., 2006): based on our *in vitro* observations, Kip3p is expected to accumulate on the growing end until there is on the order of one Kip3p molecule per protofilament.

Cooperative Depolymerization

While paused at the plus end, a single Kip3p molecule is not continuously depolymerizing the microtubule. Such continuous depolymerization would be detectable as a backward movement of a QD-labeled Kip3p. In addition, if a Kip3p removed several tubulin dimers while paused at the end, the stoichiometry would be much larger than one, in contradiction to our results. A simple picture that accounts for our observations is that when a Kip3p reaches an unoccupied protofilament end, it removes one terminal dimer and then stays bound until bumped off by an incoming Kip3p, which then removes another tubulin dimer (Figure S13A). Alternatively, the first Kip3p may not remove a tubulin dimer: in this case the incoming Kip3p would bump off a complex of the end-bound Kip3p with a tubulin dimer (Figure S13B). In either case, depolymerization is contingent on the ability of Kip3p molecules to bump each other off the end. The bump-off is most likely through a direct interaction, as evidenced from the experiments with doubly stabilized microtubules and with kinesin-1 showing that bump-off can occur without depolymerization.

Figure 7. Decrease in End-Residence Time Is Not Contingent on Microtubule Depolymerization

(A) Kymograph of Kip3p-EGFP molecules (green, 0.02 nM) moving along a doubly stabilized microtubule and pausing at the plus end in the absence of unlabeled motors. Images were recorded at 10 s intervals.

(B) Kymograph of Kip3p-EGFP molecules (green, 0.03 nM) moving along a doubly stabilized microtubule in the presence of 3.8 nM unlabeled Kip3p. The end-residence time is decreased. Images were recorded at 5 s intervals.

(C) Plot of the end-residence time (mean \pm SEM) of Kip3p-EGFP versus total concentration of Kip3p (0.03 nM Kip3p-EGFP, 0 nM to 3.8 nM unlabeled Kip3p) for doubly stabilized microtubules. The data points weighted by their SEMs were fit with a single exponential (red line). The offset is 9 s.

Thus, our experiments reveal that Kip3p depolymerizes microtubules through an unusual form of cooperativity. This mechanism accounts for the stoichiometry being approximately one.

Why does Kip3p use a cooperative mechanism to achieve depolymerization? The answer might be that Kip3p, like other walking kinesins, requires a strong-binding microtubule state for directed motility on the microtubule lattice. Thus, it cannot use the same mechanism that MCAK (kinesin-13) uses to depolymerize microtubules: MCAK uses strong binding to bend the terminal subunits and so trigger depolymerization (Moores et al., 2002) and binds only weakly to the microtubule lattice, along which it diffuses but does not walk (Helenius et al., 2006). Because the MCAK option is not available, Kip3p has found a solution using two motors; perhaps some of the work associated with the power stroke is diverted to push against the Kip3p molecule in front.

Why does Kip3p depolymerize microtubules, whereas kinesin-1 does not? The answer may be that Kip3p has a much higher affinity for the microtubule than kinesin-1. (1) Kip3p walks more slowly than kinesin-1 (50 nm/s compared to 800 nm/s), suggesting that Kip3p is slow to unbind its rear motor domain. (2) Kip3p spends >100 times longer walking on the microtubule lattice than kinesin-1. (3) Kip3p is processive at much higher salt concentrations than kinesin-1. (4) The pause of Kip3p at the microtubule end is much longer than that of kinesin-1 (~ 30 s compared to <0.3 s under the same conditions).

The high affinity of Kip3p for the microtubule could account for depolymerization as follows. When an incoming Kip3p arrives at the end, it pushes on the end-bound Kip3p. If the Kip3p-tubulin interaction is strong enough, then the force of the interaction would break the tubulin-tubulin bond before the Kip3p-tubulin bond, leading to dissociation of a Kip3p-tubulin complex. To accelerate the dissociation of tubulin 200-fold, from the spontaneous rate of 0.015 $\mu\text{m}/\text{min}$ to 3 $\mu\text{m}/\text{min}$, the activation barrier for tubulin dissociation would have to be reduced by $\ln(200)kT \approx 20 \times 10^{-21} \text{ J}$ (where kT is the Boltzmann constant times absolute temperature). Given that the energy derived from the hydrolysis of ATP under cellular conditions is $\approx 100 \times 10^{-21} \text{ J}$

(Howard, 2001), enough energy exists to power the bump-off. In this way, rather than using its energy to carry a load, Kip3p uses at least part of it to accelerate dissociation of the distal-most tubulin dimer. The fact that Kip3p has a higher microtubule lattice affinity than kinesin-1 could also account for the observed specificity of the bump-off process: kinesin-1 will dissociate before it bumps off Kip3p.

Efficiency and Signaling

Kip3p is an extraordinarily inefficient depolymerase. It takes up to a thousand steps along a microtubule, presumably hydrolyzing a thousand molecules of ATP, then it removes just a single tubulin dimer from the end before (or while) detaching. Contrast this with MCAK. MCAK targets ends by a one-dimensional diffusion on the microtubule lattice that consumes no ATP (Helenius et al., 2006). Then it removes several tubulin dimers from the end, hydrolyzing a small number of ATPs for each tubulin dimer removed (Hunter et al., 2003). The inefficiency suggests that the function of Kip3p is not just to be a depolymerase. Furthermore, a purely transport function is unlikely given that there is no evidence that Kip3p transports cellular cargos. Instead, we hypothesize that Kip3p functions as a signaling molecule. Specifically, an ensemble of Kip3p molecules uses its motor activity to collectively pace out the length of the microtubule. The read-out of the length is the depolymerase activity. Combined with length-independent growth of microtubules, this leads to length control. The set length will be modulated whenever the balance of growth and shrinkage is altered (e.g., by up- or downregulating other depolymerases or polymerases); the key feature is that by providing length feedback, the system is stable. Our experiments illustrate the general principle that the combination of motor and depolymerase activities, by kinesin-8 or kinesin-5 (Gardner et al., 2008), be it in a single molecule or in a supramolecular complex, can lead to length-dependent depolymerization. The read-out need not be depolymerization; for example, combination of a processive motor and a kinase or phosphatase could also be used to signal distance.

EXPERIMENTAL PROCEDURES

Kip3p and Kinesin-1 Expression and Purification

$\text{His}_6\text{-Kip3p}$ and $\text{His}_6\text{-Kip3p-EGFP}$ were expressed in Sf9 cells and purified as described previously (Varga et al., 2006). The concentration of active Kip3p was determined using a filter-based radiometric ATP-binding assay (Helenius et al., 2006) with ATP labeled at the α -phosphate (PerkinElmer). Kip3p concentrations are for the dimer. Reagents were purchased from Sigma unless indicated otherwise. Kinesin-1-GFP (rkin430-GFP, Rogers et al., 2001) and kinesin-1 (rkin430) were expressed in BL21(DE3) cells, purified using a combination of cation-exchange and metal-affinity chromatography, and the concentrations of dimers estimated using the Bradford assay.

GMPCPP and Doubly Stabilized Microtubules

Porcine brain tubulin was purified and rhodamine-labeled (TAMRA, Invitrogen) as previously described (Hyman et al., 1991). GMPCPP microtubules were assembled in BRB80 (80 mM PIPES/KOH, pH 6.9, 1 mM MgCl_2 , 1 mM EGTA) plus 1 mM MgGMPCPP (Jena Bioscience) containing 0.5 μM rhodamine-labeled and 1.5 μM unlabeled tubulin dimer, incubated for 2 hr at 37°C, pelleted in an Airfuge (Beckman, 28 psi, 5 min), and resuspended in BRB80 to a 0.2 μM tubulin-dimer concentration. Doubly stabilized microtubules were prepared by addition of equal volume of BRB80 containing 10 μM taxol to GMPCPP-stabilized microtubules. Ten micromolar of taxol

was present in all solutions containing doubly stabilized microtubules. The velocity and processivity of Kip3p were similar on doubly stabilized microtubules (Supplemental Experimental Procedures) as on GMPCPP microtubules.

Imaging

Microtubules, Kip3p-EGFP, and kinesin-1-GFP were imaged using a Zeiss Axiovert 200M microscope with a Zeiss 100 \times /1.45 α Plan-FLUAR objective. Images were acquired with a Metamorph (Universal Imaging) software-driven Andor DV887 iXon camera. Fluorescence excitation was provided by a mercury arc lamp coupled through an optical fiber and by a multi-line Coherent Innova 90 laser coupled to a dual port TIRF condenser (Till Photonics) or Zeiss TIRF. GFP, TRITC, and QD-655 filter sets (Chroma Technology Corp) were used to image EGFP, TAMRA, and QDs, respectively. TIRF illumination was performed at $\lambda = 488$ nm. The exposure time was 100 ms. In the kinesin-1 experiments, TIRF images were recorded continuously and overlaid on a single epifluorescence image of a microtubule.

Single-Molecule and Depolymerization Assays

Microscope chambers were constructed from coverslips, microtubules bound to the surfaces using a tubulin antibody (SAP.4G5), and the surfaces subsequently blocked with Pluronic F-127 (Helenius et al., 2006). Assays were performed in reaction solution (BRB80 supplemented with 112.5 mM KCl, 0.1 mg/ml casein, 1 mM Mg-ATP [Roche], anti-fade consisting of 10 mM DTT, 40 mM glucose, 40 $\mu\text{g}/\text{ml}$ glucose oxidase, 16 $\mu\text{g}/\text{ml}$ catalase). For the experiments in which both Kip3p-EGFP and kinesin-1 were present in the reaction chamber, the reaction solution was identical except that it contained 30 or 50 mM KCl and 100 $\mu\text{g}/\text{ml}$ glucose oxidase (Serva). For the experiments with kinesin-1 only, the reaction solution was identical except that BRB20 (same as BRB80 but with only 20 mM PIPES) was used with no added KCl and with 100 $\mu\text{g}/\text{ml}$ glucose oxidase (Serva).

Imaging Analysis

Metamorph was used for simple image processing, including microtubule length, velocity, and EGFP-intensity measurements. Analysis of the depolymerization rates, fitting the data, and modeling were performed in Igor (WaveMetrics, Lake Oswego, OR, USA). A version of the Fluorescence Object Tracking Software (Leduc et al., 2007), written in the MATLAB, was used to locate and track QDs attached to Kip3p molecules. End-residence times of Kip3p and kinesin-1 molecules were determined by counting the number of frames a molecule was present at the plus end of a microtubule and multiplying this number by the time elapsed between two frames (3.0 s to 10 s for Kip3p and 0.1 s for kinesin-1). In cases where a Kip3p molecule was present at the end for a single frame (~30% of events), this method may lead to an overestimate of the end-residence time (the maximum error is the time between consecutive frames). We did not include in our analysis microtubules with only single-frame end events.

Quantum Dot Experiments

Anti-GFP antibodies (mouse 106A20 produced by the antibody facility at MPI-CBG, Dresden, Germany) were biotinylated using the EZ-Link NHS-PEO Solid Phase Biotinylation Kit (Pierce). Ten nanomolar quantum dots (655 nm, Invitrogen) were mixed with 1 nM biotinylated anti-His (QIAGEN) or anti-GFP antibodies and incubated for 5 min. The mix was then incubated for 5 min with 0.1–1 nM $\text{His}_6\text{-Kip3p-EGFP}$ or 1 nM $\text{His}_6\text{-Kip3p}$. Finally, the mix was 25-fold diluted by the reaction solution (identical to the single-molecule experiments) and injected into the chambers containing immobilized microtubules.

Gliding Experiments

Kip3p-EGFP was bound to neutravidin-coated coverslips via biotinylated anti-GFP antibodies and the gliding of GMPCPP-stabilized rhodamine-labeled microtubules was observed in the reaction solution (Supplemental Experimental Procedures).

SUPPLEMENTAL DATA

Supplemental Data include 13 figures, Supplemental Experimental Procedures, and four movies and can be found with this article online at [http://www.cell.com/supplemental/S0092-8674\(09\)00912-X](http://www.cell.com/supplemental/S0092-8674(09)00912-X).

ACKNOWLEDGMENTS

We thank Frauke Hussmann and Burkhard Rammner for structural insights into the Kip3p motor domain, Felix Ruhnow for tracking software, and Regine Hartmann, Corina Bräuer, and Jan Ribbe for help with protein expression. We thank members of the Howard and Diez labs and Erik Schaeffer and Jonne Helenius for comments on an earlier draft of this manuscript. We acknowledge financial support by the German Ministry of Science and Education (grant 03 N 8712) and the Max Planck Society. C.L. was supported by the Gottlieb Daimler and Karl Benz Foundation and V.B. by a fellowship from the Boehringer Ingelheim Fonds.

Received: September 26, 2008

Revised: April 20, 2009

Accepted: July 10, 2009

Published: September 17, 2009

REFERENCES

- Cooper, J.R., and Wordeman, L. (2009). The diffusive interaction of microtubule binding proteins. *Curr. Opin. Cell Biol.* 21, 68–73.
- Crevenna, A.H., Madathil, S., Cohen, D.N., Wagenbach, M., Fahmy, K., and Howard, J. (2008). Secondary structure and compliance of a predicted flexible domain in kinesin-1 necessary for cooperation of motors. *Biophys. J.* 95, 5216–5227.
- Gardner, M.K., Bouck, D.C., Paliulis, L.V., Meehl, J.B., O'Toole, E.T., Haase, J., Soubry, A., Joglekar, A.P., Winey, M., Salmon, E.D., et al. (2008). Chromosome congression by Kinesin-5 motor-mediated disassembly of longer kinetochore microtubules. *Cell* 135, 894–906.
- Ghaemmaghami, S., Huh, W.K., Bower, K., Howson, R.W., Belle, A., Dephoure, N., O'Shea, E.K., and Weissman, J.S. (2003). Global analysis of protein expression in yeast. *Nature* 425, 737–741.
- Goshima, G., Wollman, R., Stuurman, N., Scholey, J.M., and Vale, R.D. (2005). Length control of the metaphase spindle. *Curr. Biol.* 15, 1979–1988.
- Grissom, P.M., Fiedler, T., Grishchuk, E.L., Nicastro, D., West, R.R., and McIntosh, J.R. (2009). Kinesin-8 from fission yeast: a heterodimeric, plus-end-directed motor that can couple microtubule depolymerization to cargo movement. *Mol. Biol. Cell* 20, 963–972.
- Gupta, M.L.J., Carvalho, P., Roof, D.M., and Pellman, D. (2006). Plus end-specific depolymerase activity of Kip3, a kinesin-8 protein, explains its role in positioning the yeast mitotic spindle. *Nat. Cell Biol.* 8, 913–923.
- Helenius, J., Brouhard, G., Kalaidzidis, Y., Diez, S., and Howard, J. (2006). The depolymerizing kinesin MCAK uses lattice diffusion to rapidly target microtubule ends. *Nature* 441, 115–119.
- Howard, J. (2001). Mechanics of Motor Proteins and the Cytoskeleton (Sunderland, MA: Sinauer Associates).
- Howard, J., and Hyman, A.A. (2007). Microtubule polymerases and depolymerases. *Curr. Opin. Cell Biol.* 19, 31–35.
- Howard, J., Hudspeth, A.J., and Vale, R.D. (1989). Movement of microtubules by single kinesin molecules. *Nature* 342, 154–158.
- Hunter, A.W., Caplow, M., Coy, D.L., Hancock, W.O., Diez, S., Wordeman, L., and Howard, J. (2003). The kinesin-related protein MCAK is a microtubule depolymerase that forms an ATP-hydrolyzing complex at microtubule ends. *Mol. Cell* 11, 445–457.
- Hyman, A., Drechsel, D., Kellogg, D., Salser, S., Sawin, K., Steffen, P., Wordeman, L., and Mitchison, T. (1991). Preparation of modified tubulins. *Methods Enzymol.* 196, 478–485.
- Hyman, A.A., Chretien, D., Arnal, I., and Wade, R.H. (1995). Structural changes accompanying GTP hydrolysis in microtubules: information from a slowly hydrolyzable analogue guanylyl-(alpha,beta)-methylene-diphosphonate. *J. Cell Biol.* 128, 117–125.
- Leduc, C., Ruhnow, F., Howard, J., and Diez, S. (2007). Detection of fractional steps in cargo movement by the collective operation of kinesin-1 motors. *Proc. Natl. Acad. Sci. USA* 104, 10847–10852.
- Marshall, W.F. (2004). Cellular length control systems. *Annu. Rev. Cell Dev. Biol.* 20, 677–693.
- Marshall, W.F., Qin, H., Rodrigo Brenni, M., and Rosenbaum, J.L. (2005). Flagellar length control system: testing a simple model based on intraflagellar transport and turnover. *Mol. Biol. Cell* 16, 270–278.
- Mayr, M.I., Hümmel, S., Bormann, J., Grüner, T., Adio, S., Woehlke, G., and Mayer, T.U. (2007). The human kinesin Kif18A is a motile microtubule depolymerase essential for chromosome congression. *Curr. Biol.* 17, 488–498.
- Moores, C.A., Yu, M., Guo, J., Beraud, C., Sakowicz, R., and Milligan, R.A. (2002). A mechanism for microtubule depolymerization by Kif1 kinesins. *Mol. Cell* 9, 903–909.
- Rogers, K.R., Weiss, S., Crevel, I., Brophy, P.J., Geeves, M., and Cross, R. (2001). KIF1D is a fast non-processive kinesin that demonstrates novel K-loop-dependent mechanochemistry. *EMBO J.* 20, 5101–5113.
- Seitz, A., and Surrey, T. (2006). Processive movement of single kinesins on crowded microtubules visualized using quantum dots. *EMBO J.* 25, 267–277.
- Straight, A.F., Sedat, J.W., and Murray, A.W. (1998). Time-lapse microscopy reveals unique roles for kinesins during anaphase in budding yeast. *J. Cell Biol.* 143, 687–694.
- Stumpff, J., von Dassow, G., Wagenbach, M., Asbury, C., and Wordeman, L. (2008). The kinesin-8 motor Kif18A suppresses kinetochore movements to control mitotic chromosome alignment. *Dev. Cell* 14, 252–262.
- Taylor, D.L., and Wang, Y.L. (1980). Fluorescently labelled molecules as probes of the structure and function of living cells. *Nature* 284, 405–410.
- Tischer, C., Brunner, D., and Dogterom, M. (2009). Force- and kinesin-8-dependent effects in the spatial regulation of fission yeast microtubule dynamics. *Mol. Syst. Biol.* 5, 250.
- Tyson, C.B., Lord, P.G., and Wheals, A.E. (1979). Dependency of size of *Saccharomyces cerevisiae* cells on growth rate. *J. Bacteriol.* 138, 92–98.
- Unsworth, A., Masuda, H., Dhut, S., and Toda, T. (2008). Fission yeast kinesin-8 Kip5 and Kip6 are interdependent for mitotic nuclear retention and required for proper microtubule dynamics. *Mol. Biol. Cell* 19, 5104–5115.
- Varga, V., Helenius, J., Tanaka, K., Hyman, A.A., Tanaka, T.U., and Howard, J. (2006). Yeast kinesin-8 depolymerizes microtubules in a length-dependent manner. *Nat. Cell Biol.* 8, 957–962.
- Wadsworth, P., and Sloboda, R.D. (1983). Microinjection of fluorescent tubulin into dividing sea urchin cells. *J. Cell Biol.* 97, 1249–1254.

Cell, Volume 138
Supplemental Data
**Kinesin-8 Motors Act Cooperatively
to Mediate Length-Dependent
Microtubule Depolymerization**

Vladimir Varga, Cecile Leduc, Volker Bormuth, Stefan Diez, and Jonathon Howard

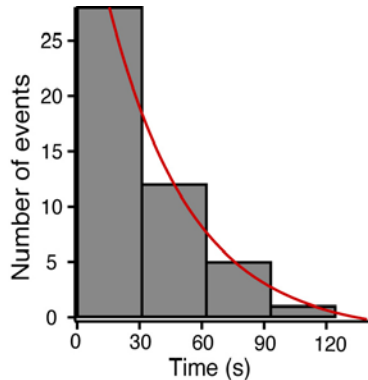


Figure S1. Duration of end-residence times of Kip3p-EGFP molecules at low total Kip3p concentrations

Histogram of duration of end-pausing events. The red line denotes an exponential fit with a time constant (i.e. the mean end-event duration) of 40 s.

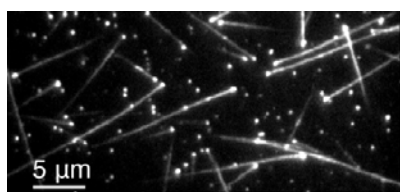


Figure S2. Kip3p-EGFP molecules pause at the plus ends of all microtubules

Average intensity projection of a movie in which single Kip3p-EGFP molecules were observed (0.01 nM Kip3p-EGFP). TIRF images were acquired every 5 s and the total duration of the movies was 11.7 min. The average intensity for each pixel was calculated using all frames of the movie. The bright dots at the microtubule plus ends indicate pausing.

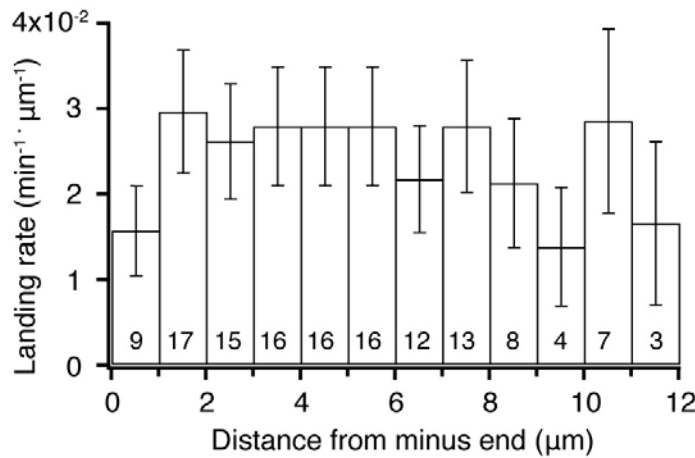


Figure S3. Landing rate of Kip3p molecules does not depend on the position along the microtubule

The landing rate of Kip3p-EGFP (0.013 nM) as a function of distance from the minus end, measured for 25 microtubules of different lengths. The number at the bottom of each bin represents the number of binding events within the 23 minute observation time, and the error bars represent SEs.

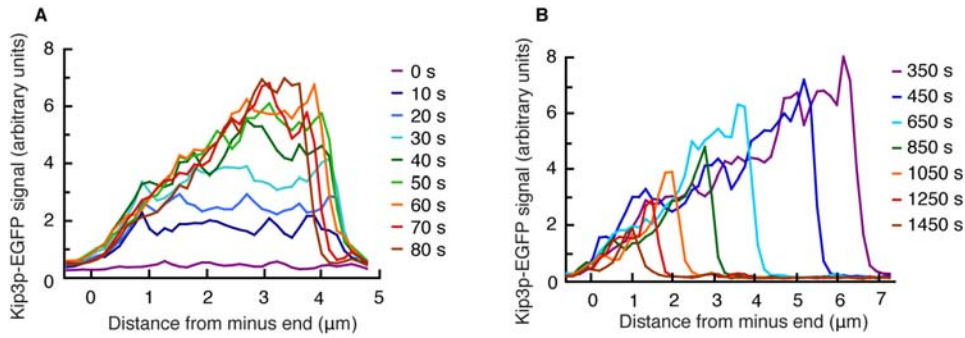
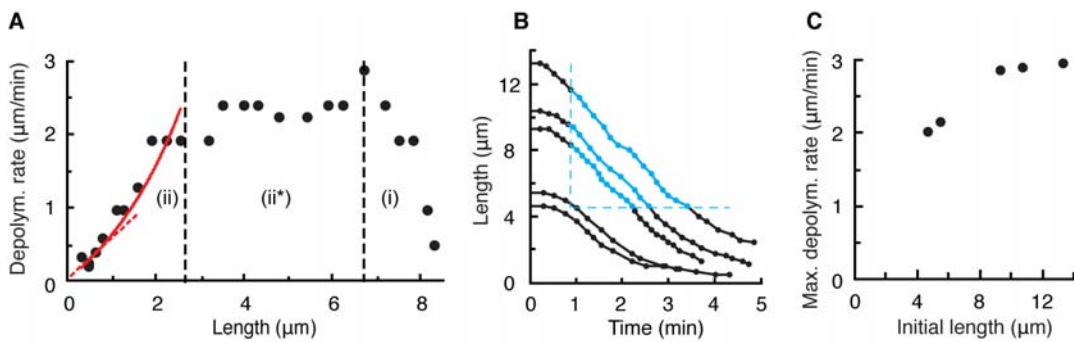


Figure S4. Kip3p-EGFP densities along the microtubule lattice during the acceleration and slow-down phases of depolymerization

A Typical graphs of Kip3p-EGFP intensity along a single microtubule during the acceleration phase (phase i). At $t = 0$ s, 2.75 nM of Kip3p-EGFP was added and images were acquired in 10-s time intervals.

B Typical graphs of Kip3p-EGFP intensity along a single microtubule during the slow-down phase (phase ii). At $t = 0$ s, 1.2 nM Kip3p-EGFP was present in the chamber.



C Maximum depolymerization rates versus initial microtubule lengths, as measured for the microtubules in B, showing saturation at lengths greater than 8 μm .

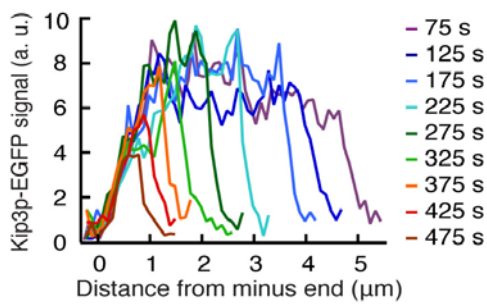


Figure S6. Kip3p-EGFP densities along the microtubule lattice during depolymerization in the high-salt buffer.

Typical graphs of Kip3p-EGFP intensity along a single microtubule after the steady-state was reached (after phase (i) was completed). At $t = 0$ s, 1.6 nM of Kip3p-EGFP was added and images were acquired in 5-s time intervals.

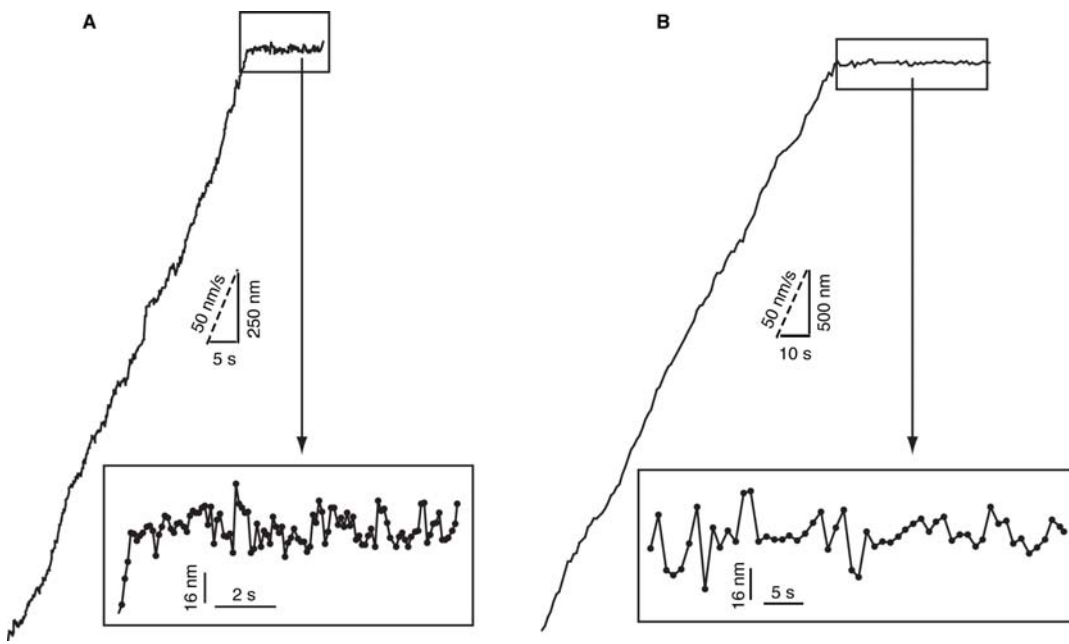


Figure S7. Control experiments with different geometries of QD-motor attachments

Walked distances of motor-attached QDs along the microtubule. Streptavidin-coated QDs were attached via biotinylated anti-GFP antibodies to the EGFP of His₆-Kip3p-EGFP (**A**) or via anti-His antibodies to the His₆ tag of His₆-Kip3p (**B**).

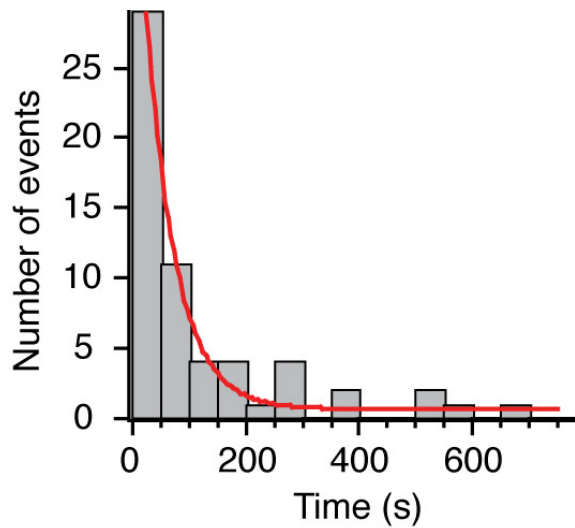


Figure S8. Duration of end events in low-density gliding assays

Histogram of time periods during which microtubules were attached with their plus ends to a surface-bound Kip3p motor and performed pivotal swiveling. The red line denotes an exponential fit with a time constant (i.e. the mean end-event duration) of 52 ± 5 s (SE).

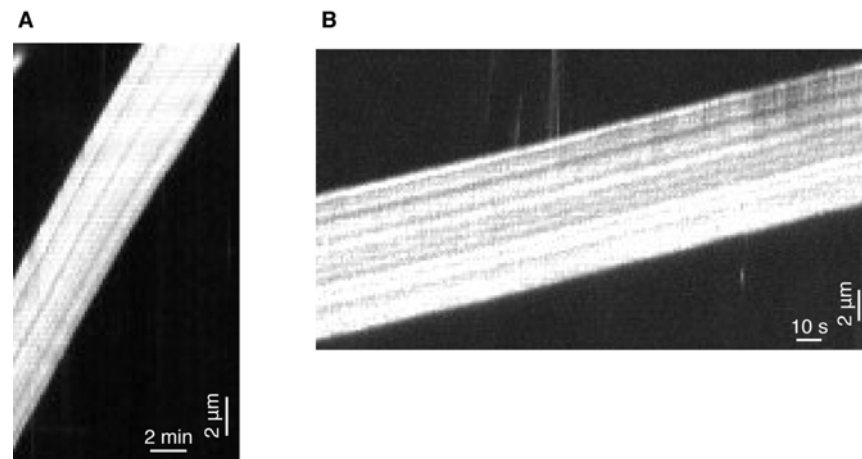


Figure S9. Microtubule motility in high-density gliding assays

Kymographs showing the motility of microtubules driven by surface-bound Kip3p-EGFP. Epifluorescence images were recorded every 10 s (**A**) and 1 s (**B**).

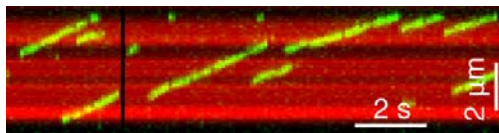


Figure S10. In buffers having physiological ionic strength, kinesin-1 does not dwell noticeably at the plus end

Kymograph showing the movement of single kinesin-1-GFP molecules along the lattice of a microtubule. TIRF images were recorded continuously and overlaid on a single epifluorescence image of a microtubule. The black line indicates a part of the movie, in which no kinesin-1 molecules were present on the microtubule, that was removed.

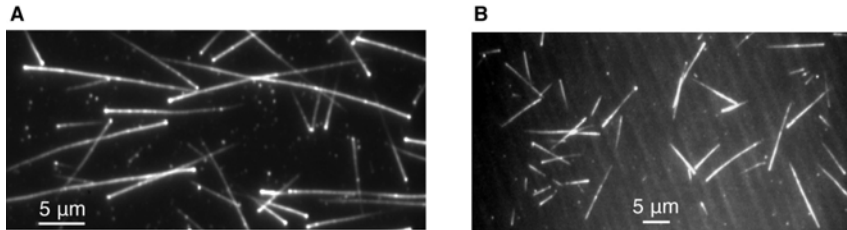


Figure S11. In low-ionic-strength buffers, kinesin-1-GFP molecules pause at the plus end of all microtubules and the end-residence time is decreased in the presence of unlabeled kinesin-1

(A) Average intensity projection of a movie at low kinesin-1-GFP concentration (0.5 nM). TIRF images were acquired at 1-s intervals and the total duration of the movies was 4 min. The average intensity for each pixel was calculated using all frames of the movie. Note the bright dots at the microtubule plus ends, indicating pausing.

(B) Average intensity projection of a movie from the experiment in which 0.02 nM kinesin-1-GFP and 3 nM unlabeled kinesin-1 was present. TIRF images were acquired continuously and the total duration of the movies was 40 s. The average intensity for each pixel was calculated using all frames of the movie. Note the absence of the bright dots at the microtubule plus ends, indicating that bump-off has occurred.

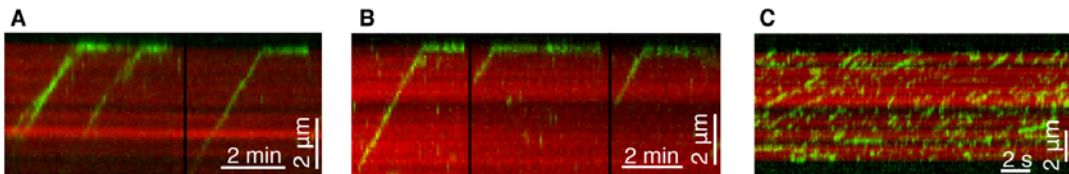


Figure S12. Kinesin-1 does not decrease the end-residence time of Kip3p

(A) Kymograph showing behavior of single Kip3p-EGFP molecules (0.8 nM) on a GMPCPP-stabilized microtubule in the reaction solution based on BRB80 with 50 mM KCl (See methods). Molecules traveled on average $17.8 \pm 6.7 \mu\text{m}$ (SE, $N = 7$ detachments), with the average velocity of $2.1 \pm 0.2 \mu\text{m/min}$ (SD, $N = 23$), and after reaching the plus end they paused there on average for $77 \pm 47 \text{ s}$ (SD, $N = 19$). Images were recorded at 5 s intervals. The black line indicates a part of the movie, in which no Kip3p-EGFP molecules were present on the microtubule, that was removed.

(B) Kymograph showing the behavior of single Kip3p-EGFP molecules (0.8 nM) on a microtubule in the reaction solution based on BRB80 with 50 mM KCl in the presence of 13 nM unlabeled Kinesin-1. Kip3p-EGFP molecules traveled on average $16.5 \pm 4.6 \mu\text{m}$ (SE, $N = 13$ detachments), with the average velocity of $2.2 \pm 0.4 \mu\text{m/min}$ (SD, $N = 48$), and after reaching the plus end they paused there on average for $100 \pm 54 \text{ s}$ (SD, $N = 17$). Images were recorded at 5 s intervals. The black lines indicate a part of the movie, in which no Kip3p-EGFP molecules were present on the microtubule, that was removed. The flux of kinesin-1 molecules (as estimated from similar experiments with GFP-labeled kinesin-1, see (C)) was ~2 molecules per protofilament end per minute. In similar experiments with 30 mM KCl, the end-residence time was $340 \pm 310 \text{ s}$ (SD, $N = 16$) without kinesin and $280 \pm 240 \text{ s}$ (SD, $N = 35$) when the kinesin flux was ~3 molecules per protofilament end per minute. These experiments show that the probability of a kinesin-1 bumping off a Kip3p is less than 10% and 3% respectively.

(C) Kymograph showing that kinesin-1-GFP molecules reach the plus ends of microtubules in the same buffer as used in (B). 17 nM kinesin-1-GFP was present in the reaction chamber. TIRF images were recorded continuously and overlaid on a single epifluorescence image of a microtubule.

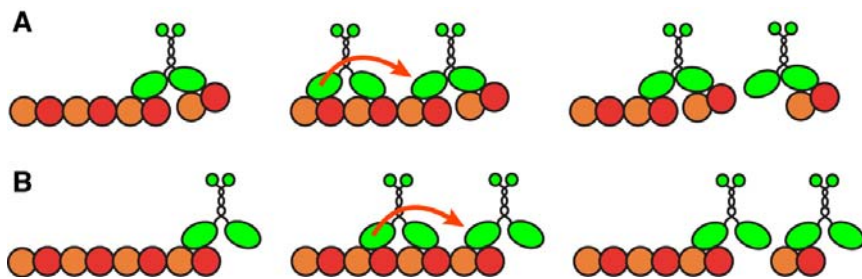


Figure S13. Bump-off mechanisms that could explain the accelerated detachment of end-bound Kip3p by incoming motors

(A) Tubulin removal before bump-off: After Kip3p reaches a vacant end, it severs the interdimer bond, perhaps due to intramolecular strain developed when both motor domains are tightly bound (left). An incoming Kip3p then bumps off the end-bound one. This acceleration of Kip3p detachment from the plus end occurs due to competition for the Kip3p-binding site on the penultimate tubulin dimer (middle). The binding of the second Kip3p molecule to the end is then followed by another severing (right).

(B) Tubulin removal during bump-off: A Kip3p molecule binds stably to the terminal tubulin dimer at the microtubule's plus end (left). An incoming Kip3p bumps into the paused molecule (middle) causing severing and dissociation of a Kip3p-tubulin complex (right).

Supplemental Experimental Procedures

Doubly stabilized microtubules. The velocity and processivity of Kip3p were similar on doubly stabilized microtubules (low-concentration experiments: velocity $3.0 \pm 0.4 \mu\text{m}/\text{min}$, SD, $N = 40$; run length $19 \pm 8 \mu\text{m}$ (SE), $N = 6$ detachments; high-concentration spiking experiments: velocity $3.0 \pm 0.04 \mu\text{m}/\text{min}$, SD, $N = 33$ molecules; run length $11 \pm 4 \mu\text{m}$ (SE) $N = 9$ detachments) as on GMPCPP microtubules.

Gliding experiments. Chambers were incubated for 10 min with 0.1 mg/ml neutravidin in PBS, followed by a rinse with 20 μl of BRB80. After 5 min incubation with 1% Pluronic F-127 in BRB80 and a rinse (60 μl of BRB80), the chambers were perfused with PBS containing 0.3 mg/ml casein and biotinylated anti-GFP antibodies (final concentration 0.075 mg/ml for low-density and 1.5 mg/ml for high-density assays) and biotin was allowed to interact with neutravidin for 20 min. To remove unbound antibodies the chambers were rinsed with 80 μl of BRB80 and 20 μl of washing solution (BRB80 supplemented with 112.5 mM KCl, 0.8 mg/ml casein and 1 mM Mg-ATP). 4 nM His₆-Kip3p-EGFP in 50 mM NaPO₄ buffer pH 7.5 supplemented with 300 mM NaCl, 300 mM imidazole, 10 % glycerol, 1 mM MgCl₂, 10 μM Mg-ATP, 0.2 mg/ml casein and 0.1% Tween 20 was incubated in the chambers for 10 min, followed by 20 μl rinse with the washing solution. Finally, GMPCPP-stabilized rhodamine-labeled microtubules (0.02 μM tubulin-dimer concentration) in the reaction solution (identical to the single-molecule experiments) were added and the chambers were sealed with vacuum grease.

Mathematical Formulation of the Antenna model

We developed a mathematical formulation of the antenna model to describe the depolymerization rate of a microtubule as a function of the flux of Kip3p to the plus end. The model assumes that (i) Kip3p molecules bind randomly along the length of the microtubule (with landing rate r), (ii) all molecules walk to the end (i.e. very high processivity) with velocity v and (iii) they remove n subunits from the end (n is the stoichiometry).

Simplified binding model. To simplify the mathematics, we initially assume that the landing rate is independent of the lattice occupancy (defined as the number

of Kip3p dimers per tubulin dimer) until saturation occurs. Later, we will solve the more exact model, which takes into account the number of free sites on the lattice on the landing rate. However, the solutions are similar.

The depolymerization rate, v_- is given by:

$$v_- = -\frac{dL}{dt} = nd\rho(L)v + nd\rho(L)v_- = nd\rho(L)[v + v_-] \quad (1)$$

where L is the microtubule length (distance from the minus end to the plus end) at time t , d is the change of microtubule length corresponding to the removal of one tubulin dimer ($d = 0.6$ nm), and ρ is the density of Kip3p along the microtubule lattice (the occupancy equals ρd). The term nd is the change in the microtubule length due to the activity of a single Kip3p molecule reaching the end, while the term $\rho(L)(v+v_-)$ defines the flux of Kip3p molecules to the plus end. The flux has two components: $\rho(L)v$ due to the movement of Kip3p along the microtubule lattice and $\rho(L)v_-$ due to the shortening of the microtubule, which brings the end toward the incoming Kip3p molecules. The sum $v+v_-$ can be considered the relative velocity at which a Kip3p molecule approaching the plus end of a depolymerizing microtubule. Notice that due to the term $nd\rho(L)v$, which plays the role of positive feedback, the depolymerization rate is not linearly dependent on the length of a microtubule.

If Kip3p is added to a microtubule of initial length L_0 , we can identify three regimes of microtubule shrinkage:

(i) At early times, the density of Kip3p increases linearly from zero at the minus end to a value rt , and then remains constant to the plus end.

$$\rho(x) = \begin{cases} \frac{rx}{v} & x \leq vt \\ rt & x \geq vt \end{cases} \quad t \leq t_1$$

t_1 is the time at which the linear gradient first extends to the end of the microtubule. Substituting $\rho(L) = rt$ in Equation 1 and solving for v_- we obtain

$$v_- = -\frac{dL}{dt} = v \frac{ndrt}{1 - ndrt} \quad (2)$$

Integration of Equation 2 gives:

$$L(t) = \frac{v}{ndr} \left[\ln(1 - ndrt) + ndrt \right] + L_0 \quad t \leq t_1 = \frac{v}{L(t_1)} \quad (3)$$

(ii*) At intermediate times, the Kip3p density may saturate on the microtubule lattice. Suppose that the maximum Kip3p density is $\rho_{\max} = rt_1$ and is reached at time t_1 . Then,

$$\rho(x) = \begin{cases} \frac{rx}{v} & x \leq vt_1 \\ \rho_{\max} & x \geq vt_1 \end{cases} \quad t_1 \leq t \leq t_2$$

This equation is used to model the density profiles shown in Figure 3F. In this saturation phase,

$$v_- = v \frac{nd\rho_{\max}}{1 - nd\rho_{\max}} = v_-^{\max} \quad (4)$$

(ii) After the saturated region of the microtubule has been depolymerized (at time t_2), the concentration profile is constant over time and linear over distance

$$\rho(x) = \frac{rx}{v} \quad t \geq t_2$$

During this slow-down phase

$$v_- = -\frac{dL}{dt} = v \frac{ndrL / v}{1 - ndrL / v} \quad (5)$$

This equation is used for the solid curve in Figure 3B and Supplementary Figure 5A. As the microtubule length approaches zero, the denominator approaches 1, so that there is a linear relationship between the depolymerization rate and the microtubule length (dashed curve in Figure 3B). The slope, denoted ‘final slope’, is $ndr = ndk_{\text{on}}[\text{Kip3p}]$, where k_{on} is the measured second order association rate per unit length of microtubule (Figure 3C).

Integration of Equation 5 gives:

$$t = t_2 + \frac{L - L_2}{v} - \frac{1}{ndr} \ln \frac{L}{L_2} \quad t \geq t_2 \quad (6)$$

where $L_2 = L(t_1) - v_-^{\max} (t_2 - t_1)$. Equations (3) and (6) are used in the fit in Figure 3A. Equations (3), (4) and (6) are used in the fit in Figure 3D.

Gradual binding model. A more realistic model of microtubule depolymerization takes into account the gradual decrease in the landing rate of Kip3p as the occupancy of Kip3p on the lattice increases. The landing rate r then becomes non-uniform along the lattice as it depends on the Kip3p density ρ :

$$r(\rho) = k_{\text{on}}[\text{Kip3p}] \left(1 - \rho / \rho_{\max}\right) \quad (7)$$

When Kip3p is added to a microtubule of initial length L_0 , the density of Kip3p along the lattice can be derived from the differential equation:

$$\frac{\partial \rho}{\partial t}(x, t) = -v \frac{\partial \rho}{\partial t}(x, t) + r(\rho) \quad (8)$$

The Kip3p density profile after the initial acceleration phase (phase (i) in the simplified model) is then:

$$\rho(x) = \rho_{\max} \left(1 - \exp\left(-\frac{r_0 x}{v \rho_{\max}}\right) \right) \quad (9)$$

where r_0 is the landing rate on a naked microtubule ($\rho=0$). For $x = v \rho_{\max} / r_0$, we obtain $\rho(x) = r_0 x / v$, equivalent to the result in the simplified model.

The depolymerization rate v is obtained from Equation (1):

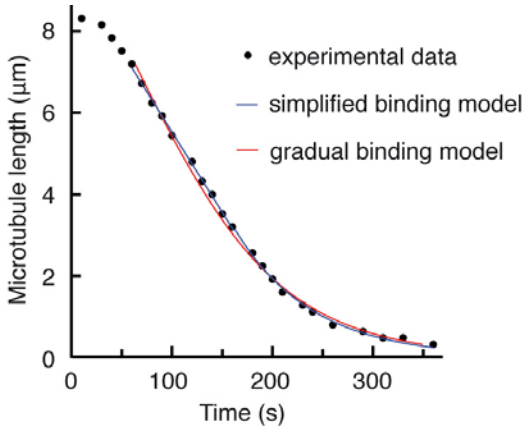
$$v_- = -\frac{dL}{dt} = v \frac{nd\rho(L)}{1 - nd\rho(L)} \quad (10)$$

Using Equations (9) and (10), we deduce the depolymerization curve:

$$t - t_1 = \left(\frac{1}{v} - \frac{1}{nd\rho_{\max} v} \right) (L - L_1) - \frac{1}{r_0 nd} \ln \left\{ 1 - \exp \left[-\frac{r_0 (L - L_1)}{v \rho_{\max}} \right] \right\} \quad (11)$$

for $t > t_1$, when the steady-state is established at the length L_1 .

Using Equation (11), we can fit the depolymerization curve of Figure 3D. The comparison of the fit obtained with the gradual binding model and the simplified binding model is shown in the following figure:



Both models give similar values for ndr , from which we deduced estimations of the stoichiometry n . Our experimental data are not precise enough to distinguish between both models. Therefore, we decided to use the simplified binding model in the text.